The Astrophysical Journal Letters, 809:L12 (7pp), 2015 August 10 doi:10.1088/2041-8205/809/1/L12

MURCHISON WIDEFIELD ARRAY OBSERVATIONS OF ANOMALOUS VARIABILITY: A SERENDIPITOUS NIGHT-TIME DETECTION OF INTERPLANETARY SCINTILLATION

D. L. Kaplan[1], S. J. Tingay[2,3], P. K. Manoharan[4], J. P. Macquart[2,3], P. Hancock[2,3], J. Morgan[2], D. A. Mitchell[3,5], R. D. Ekers[5], R. B. Wayth[2,3], C. Trott[2,3], T. Murphy[3,6], D. Oberoi[4], I. H. Cairns[6], L. Feng[7], N. Kudryavtseva[2], G. Bernardi[8,9,10], J. D. Bowman[11], F. Briggs[12], R. J. Cappallo[13], A. A. Deshpande[14], B. M. Gaensler[3,6,15], L. J. Greenhill[10], N. Hurley Walker[2], B. J. Hazelton[16], M. Johnston Hollitt[17], C. J. Lonsdale[13], S. R. McWhirter[13], M. F. Morales[16], E. Morgan[7], S. M. Ord[2,3], T. Prabu[14], N. Udaya Shankar[14], K. S. Srivani[14], R. Subrahmanyan[3,14], R. L. Webster[3,18], A. Williams[2], and C. L. Williams[7]

[1] Department of Physics, University of Wisconsin–Milwaukee, Milwaukee, WI 53201, USA; kaplan@uwm.edu
[2] International Centre for Radio Astronomy Research, Curtin University, Bentley, WA 6102, Australia
[3] ARC Centre of Excellence for All-sky Astrophysics (CAASTRO)
[4] Radio Astronomy Centre, National Centre for Radio Astrophysics, Tata Institute of Fundamental Research, Ooty 643001, India
[5] CSIRO Astronomy and Space Science (CASS), P.O. Box 76, Epping, NSW 1710, Australia
[6] Sydney Institute for Astronomy, School of Physics, The University of Sydney, NSW 2006, Australia
[7] Kavli Institute for Astrophysics and Space Research, Massachusetts Institute of Technology, Cambridge, MA 02139, USA
[8] SKA SA, 3rd Floor, The Park, Park Road, Pinelands 7405, South Africa
[9] Department of Physics and Electronics, Rhodes University, P.O. Box 94, Grahamstown 6140, South Africa
[10] Harvard-Smithsonian Center for Astrophysics, Cambridge, MA 02138, USA
[11] School of Earth and Space Exploration, Arizona State University, Tempe, AZ 85287, USA
[12] Research School of Astronomy and Astrophysics, Australian National University, Canberra, ACT 2611, Australia
[13] MIT Haystack Observatory, Westford, MA 01886, USA
[14] Raman Research Institute, Bangalore 560080, India
[15] Dunlap Institute for Astronomy and Astrophysics, University of Toronto, 50 St. George Street, Toronto, ON M5S 3H4, Canada
[16] Department of Physics, University of Washington, Seattle, WA 98195, USA
[17] School of Chemical and Physical Sciences, Victoria University of Wellington, Wellington 6140, New Zealand
[18] School of Physics, The University of Melbourne, Parkville, VIC 3010, Australia
Received 2015 April 17; accepted 2015 July 23; published 2015 August 7

ABSTRACT

We present observations of high-amplitude rapid (2 s) variability toward two bright, compact extragalactic radio sources out of several hundred of the brightest radio sources in one of the 30° × 30° Murchison Widefield Array (MWA) Epoch of Reionization fields using the MWA at 155 MHz. After rejecting intrinsic, instrumental, and ionospheric origins we consider the most likely explanation for this variability to be interplanetary scintillation (IPS), likely the result of a large coronal mass ejection propagating from the Sun. This is confirmed by roughly contemporaneous observations with the Ooty Radio Telescope. We see evidence for structure on spatial scales ranging from <1000 to $>10^6$ km. The serendipitous night-time nature of these detections illustrates the new regime that the MWA has opened for IPS studies with sensitive night-time, wide-field, low-frequency observations. This regime complements traditional dedicated strategies for observing IPS and can be utilized in real-time to facilitate dedicated follow-up observations. At the same time, it allows large-scale surveys for compact (arcsec) structures in low-frequency radio sources despite the 2′ resolution of the array.

Key words: radio continuum: galaxies – scattering – Sun: coronal mass ejections (CMEs) – Sun: heliosphere – techniques: interferometric

1. INTRODUCTION

Interplanetary scintillation (IPS)—the rapid (<1–10 s) flux density variability of distant compact radio sources due to radio-wave propagation through inhomogeneities in the ionized solar wind—was discovered by Clarke (1964) and published by Hewish et al. (1964); the discovery led to high-time-resolution instrumentation that, in turn, led to the discovery of pulsars (Hewish et al. 1968). IPS is an important technique in monitoring the structure and evolution of the solar wind (e.g., Coles 1978; Manoharan & Ananthakrishnan 1990; Jackson et al. 1998), particularly as a probe of major perturbations caused by solar flares and Coronal Mass Ejections (CMEs; e.g., Tokumaru et al. 2003; Manoharan 2010), and in constraining the nature of background radio sources (Little & Hewish 1968).

Observations of IPS are typically made at low radio-frequencies, <400 MHz, where the effects of plasma inhomogeneities are most apparent. At facilities such as the Ooty radio telescope (Manoharan 2010), the Mexican Array Radio Telescope (Mejia-Ambriz et al. 2010), and the Solar Wind Imaging Facility, Toyokawa (Tokumaru et al. 2011)/Solar-Terrestrial Environment Laboratory (Kojima & Kakinuma 1990), observations measure the modulation of hundreds of pre-selected radio sources each day and follow solar-wind events identified elsewhere. The new generation of low-frequency, wide-field radio telescopes such as the Murchison Widefield Array (MWA; Lonsdale et al. 2009; Tingay et al. 2013) and Low Frequency Array (LOFAR; van Haarlem et al. 2013) can undertake both dedicated observations of IPS (Oberoi & Benkevitch 2010; Bisi et al. 2011; Fallows et al. 2013)—often at high time resolution—and make serendipitous discoveries, as discussed here. These ground-based radio IPS facilities complement space-based heliospheric imagers such as *STEREO* (Eyles et al. 2009), *SDO* (Schou

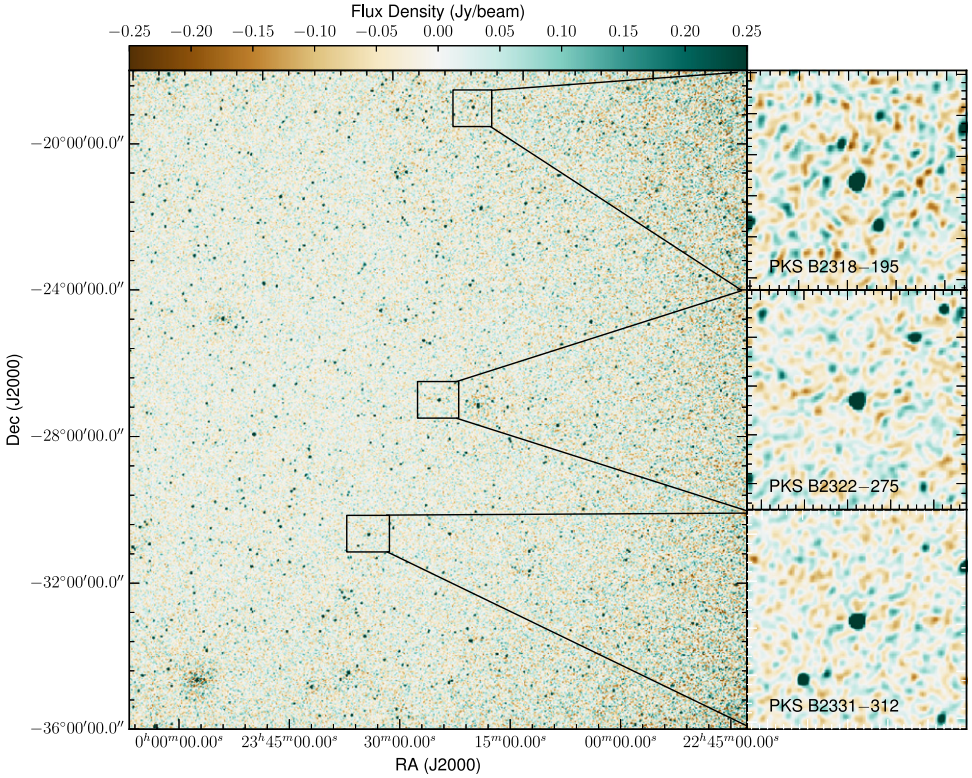

Figure 1. MWA 155 MHz image of the EoR0 field, centered on PKS B2322−275. The image is a single 2 minute integration from 2014 November 6 and is roughly 17° on a side. We show 1 deg^2 boxes around PKS B2322−275, PKS B2318−195, and PKS B2331−312, with expanded views around these sources in the insets to the right.

et al. 2012), and *Hinode* (Culhane et al. 2007), and in situ solar wind measurements from other spacecraft.

The MWA is a low frequency (80–300 MHz) interferometer located in Western Australia, with solar, heliospheric, and ionospheric studies as one of its major focuses (Bowman et al. 2013). The advantages of the MWA for IPS are: its southern hemisphere location (all major IPS facilities are in the northern hemisphere); its very wide field of view (over 600 deg^2 at 150 MHz); its high sensitivity for short integrations (∼100 mJy/beam rms for a 1 s integration); and its capability to make sub-second flux density measurements. Here we present the first serendipitous, exploratory observations of IPS using the MWA in its normal imaging mode with 2 s time resolution.

2. OBSERVATIONS AND DATA ANALYSIS

Data for this investigation were from commensal MWA proposals[19] G0009 ("Epoch of Reionisation, EoR") and G0005 ("Search for Variable and Transient Sources in the EoR Fields with the MWA"). The observations are of one of the MWA EoR fields (designated EoR0, and centered at J2000 R.A. $= 0^h$, decl. $= -27°$; see Figure 1) and occurred between 11:30 and 14:14 UT on 2014 November 6, while the field was within approximately two hours of transit. The observations (see Loi et al. 2015a for more details) used 40 kHz fine channels across a 30.72 MHz bandwidth centered at 155 MHz and 2 s integrations; the correlated data were written to files of 2 minutes each, with gaps of 16–24 s between adjacent files.

[19] http://www.mwatelescope.org/astronomers

Images were searched for Fast Radio Bursts (Lorimer et al. 2007; Thornton et al. 2013) using a processing pipeline which will be described elsewhere (Tingay et al. 2015). A by-product of this processing is the total power variability for every object in the MWA field of view at 2 s cadence. Very strong detections were triggered at the position of PKS B2322−275 (a redshift 1.27 quasar; McCarthy et al. 1996) during a two minute period (13:30:00–13:32:00 UT). This variability prompted the detailed follow-up analysis described below.

2.1. Real-time System Analysis

Once the initial variability from PKS B2322−275 was identified, we searched for variability from other objects in the field. We analyzed data from the MWA Real-time System (RTS; Mitchell et al. 2008; Tingay et al. 2013), which derives calibration solutions including flux densities for hundreds of sources over the MWA field of view during each integration. For each of the sources measured by the RTS (down to 155 MHz flux densities of about 1 Jy/beam, depending on the position in the MWA primary beam) we examined the modulation during the observation. Most of the sources had no substantial excess variability (confirming the results of Bell et al. 2014 and Hurley-Walker et al. 2014). However, we did identify a second source that had significant (>30% over a 2 minute interval) modulation, which we identified as PKS B2318−195. We focus on these two sources; both are bright and have no nearby neighbors to corrupt the flux density measurements (Figure 1).

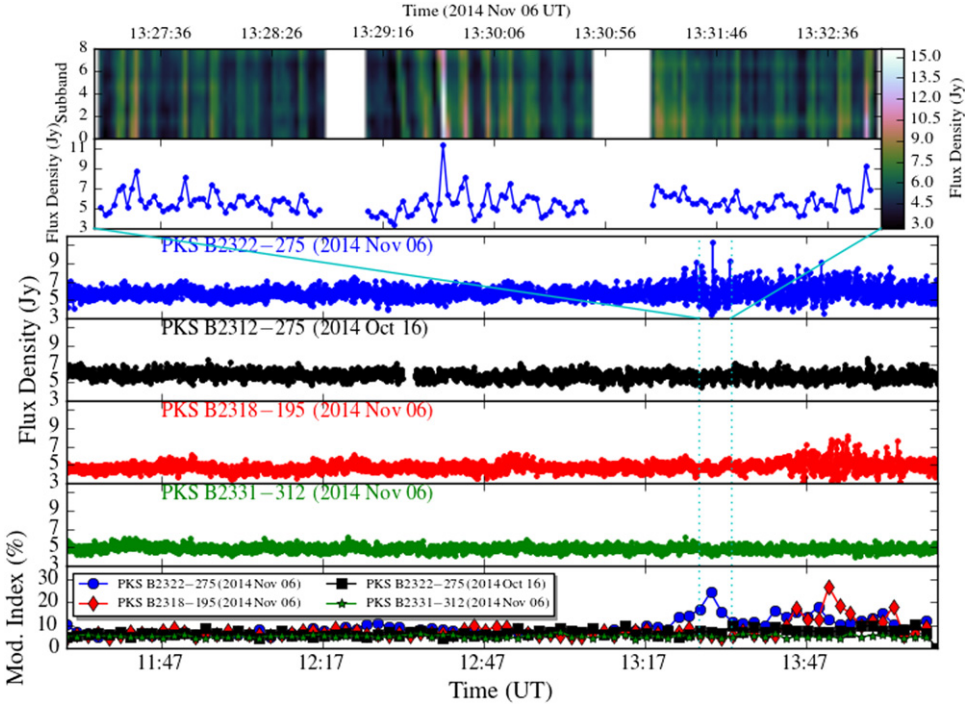

Figure 2. Bottom section: flux densities of PKS B2322−275 on 2014 November 6 (blue), PKS B2322−275 on 2014 October 6 (black), PKS B2318−195 on 2014 November 6 (red), and PKS B2331−312 on 2014 November 6 (green) measured with the MWA. The flux densities were measured from individual 2 s integrations, with uncertainty of about 0.2 Jy. Note that the *y*-axis ranges for all four panels are the same. Bottom panel: the modulation index (rms flux density variation over a 2 minute interval divided by the average flux density for that interval) for the same data sets. The expected uncertainty on the modulation index under the assumption of no extra variability is <1%. The top section shows the flux density of PKS B2322−275 along with the dynamic spectrum, measuring the flux density across eight different sub-bands (3.84 MHz each, with frequency increasing from the bottom) for the period indicated. The gaps are from the intervals between subsequent 2 minute observations.

2.2. *Imaging Analysis*

To refine our analysis, we retrieved the observations from 2014 November 6 11:30 UT to 06 14:14 UT from the MWA archive. The processing followed standard MWA procedures (e.g., Hurley-Walker et al. 2014). We calibrated the data using an observation of 3C 444, then rotated the phases of the visibilities to center the field on PKS B2322−275. We imaged individual 2 s integrations in the XX and YY instrumental polarizations using `WSClean` (Offringa et al. 2014), performing 200 `CLEAN` iterations on each and making images with 3072 × 3072 0.′45 pixel, with synthesized beam full-width at half maximum of 2.′3. Finally, we corrected the instrumental polarization to Stokes I (total intensity) using the primary beam from Sutinjo et al. (2015). For a single 2 s integration, the average image noise was 0.16 Jy/beam. In Figure 1 we show a 2 minute integration with a slightly wider field of view, which has a rms noise of about 0.05 Jy/beam.

We then used `Aegean` (Hancock et al. 2012) to measure the flux densities and positions of PKS B2322−275, PKS B2318−195, and a number of other sources with comparable (4–10 Jy) flux densities. Both targets had mean flux densities consistent with catalog values (5.8 Jy at 160 MHz for PKS B2322−275, and 4.8 Jy at 155 MHz for PKS B2318−195; Slee 1995; Hurley-Walker et al. 2014). For each integration we determined the mean fractional variation—caused by residual instrumental/ionospheric effects—of a number of other sources and divided it from each integration. We plot the resulting time series in Figure 2. We also show the modulation index (rms divided by mean over a 2 minute interval) for PKS B2322−275 and PKS B2318−195. For comparison, we plot the flux densities of one of the reference sources (PKS B2331−312, also shown in Figure 1) and of PKS B2322−275 on another night with a comparable data set (2014 October 16, chosen randomly). During the quiescent periods both PKS B2322−275 and PKS B2318−195 have modulation comparable to that for the reference source and PKS B2322−275 on the comparison night (roughly 5%, consistent with the measured noise properties). But at the peak, both PKS B2322−275 and PKS B2318−195 show modulation of >100% peak-to-peak on 2 s timescales, corresponding to rms variations of >25% averaged over 2 minutes. For PKS B2322−275 we see that the brightest spike occurs first at the upper edge of the bandpass before progressing down, giving large apparent swings in the instantaneous spectral index. The variations for PKS B2322−275 appear roughly 20 minutes before those in PKS B2318−195, which is about 9° north of PKS B2322−275 and at a slightly higher solar elongation ($\epsilon = 114°$ for PKS B2322−275 versus $\epsilon = 118°$ for PKS B2318−195) appears to start 20–30 minutes after that for PKS B2322−275. There is no indication of increases in the amplitude of position fluctuations during the period of most intense variability, with fluctuations of about 5″.

In Figure 3 we show temporal power spectra for PKS B2322−275 and PKS B2318−195 (again with PKS B2331−312 and with PKS B2322−275 from another night for comparison) created from the parts of Figure 2 with strong variability. Both PKS B2322−275 and PKS B2318−195 have considerably more power at frequencies above roughly 0.06 Hz than the comparison observation. Below this point the power spectra are similar, suggesting that this is the transition to "normal"

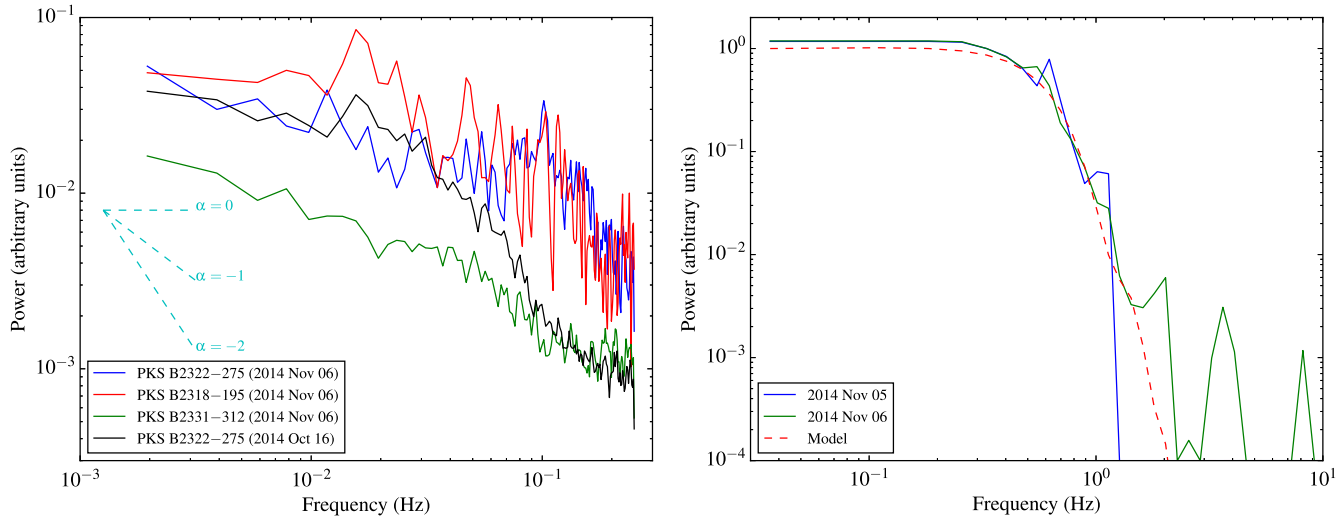

Figure 3. Left: temporal power spectra of the flux densities for PKS B2322−275 (blue, with 62 minutes of data), PKS B2318−195 (red, with 37 minutes of data), and PKS B2331−312 (green, with 235 minutes of data), using the data from Figure 2 when large-amplitude scintillations are evident. The power spectra are estimated using Welch's method, averaging spectra with 256 data-points and 50% overlap. We also show the power spectrum of PKS B2322−275 from our comparison night (black). The cyan dashed lines show power-laws with slopes $\alpha = 0, -1$, and -2 as labeled. Right: temporal power spectra of the flux density for PKS B2211−388, measured by the Ooty radio telescope at 327 MHz. The power spectrum for 2014 November 5 (blue) shows substantially less power above 1 Hz than that for 2014 November 6 (green; note that both power spectra have been normalized below 0.1 Hz). The model fit (red dashed line) is for a solar wind velocity of ≈500 km s^{-1}.

variability (likely dominated by the ionosphere, which should affect all sources roughly equally). Above the transition both scintillating sources are similar, declining with spectral slopes of roughly 1.

3. DISCUSSION

3.1. Origin of Variability

We can reject intrinsic variability since it appears for more than one source at roughly the same time. Moreover, light travel time arguments for an active galactic nucleus (AGN) rule out the 2 s timescale we see, and the extreme apparent spectral swings do not resemble any known source behavior. Instrumental effects are also ruled out, since the timescales for instrumental changes (30 minutes) are far longer than the fluctuations we see and only two sources vary. We are then left with propagation effects, i.e., scintillation due to inhomogeneous, turbulent plasma along the line of sight. We must consider whether scintillation is of interstellar, interplanetary, or ionospheric origin.

Refractive interstellar scintillation causes much slower (minutes to months) tens-of-percent variations in the flux densities of compact radio sources, with the timescale increasing at lower frequencies (e.g., Rickett 1986), hence can be clearly ruled out. Diffractive scintillation can be substantially faster (Cordes & Rickett 1998), but would require sizes that imply brightness temperatures of $\gg 10^{12}$ K—impossible for an AGN (Readhead 1994).

Ionospheric scintillation affects sources with angular sizes $\lesssim 10'$ (Loi et al. 2015b), causing joint position and amplitude fluctuations on timescales of $\gtrsim 20$ s (Thompson et al. 2001), with the former a significant source of position wander in MWA data (Hurley-Walker et al. 2014; Loi et al. 2015b) and the latter usually not very significant (although see Fallows et al. 2014). Therefore, ionospheric refraction should affect the thousands of unresolved sources in each image. In contrast, here the very strong amplitude fluctuations without any position shifts for unresolved sources and the rather small number of scintillating sources argue strongly against scattering by ionospheric plasma.

In contrast, IPS requires significant source structure on scales $<1''$ (Hewish et al. 1964; Little & Hewish 1968). All three sources discussed here are regularly monitored for IPS with Ooty: both PKS B2322−275 and PKS B2318−195 are often seen to scintillate with Ooty, consistent with angular sizes of $\lesssim 0.''1$ (at 327 MHz), while Ooty sees very little (if any) scintillation toward PKS B2331−312. Note that Ooty does not observe past $\epsilon = 100°$, so it could not monitor PKS B2322−275 during this event, although it did observe a number of nearby sources at $\epsilon > 90°$ (Figures 3 and 4) that showed enhanced scintillation on 2014 November 6 at frequencies >2 Hz.

Moreover, the two scintillating sources are detected at frequencies up to 20 GHz (Murphy et al. 2010), suggesting the presence of compact structure[20] (Chhetri et al. 2013). In contrast, PKS B2331−312 has a similar flux density at 155 MHz (Hurley-Walker et al. 2014) but is not detected above 5 GHz (implying a steeper spectral index $\alpha \approx -1.2$, with $S_\nu \propto \nu^\alpha$) and hence likely has more extended emission. This can explain why PKS B2322−275 and PKS B2318−195 were observed to be the only significant bright scintillators. That would not be the case for an ionospheric origin.

Finally, NASA's Omniweb database[21] suggests that only weak auroral and ionospheric activity occurred on both nights, with no clear CME arriving at Earth, modest K_p indices[22] (global average magnetic activity) of about 2, and temporal behavior over the whole field typical of quiet ionospheric

[20] PKS B2322−275 is one of only two sources in this field brighter than 5 Jy at 180 MHz which is unresolved at 20 GHz (determined by its 6 km baseline flux density). PKS B2318−195 is partially resolved at 20 GHz, suggesting some arcsecond-scale structure but also significant compact emission.

[21] See http://omniweb.gsfc.nasa.gov/.

[22] See http://www.ngdc.noaa.gov/stp/GEOMAG/kp_ap.html.

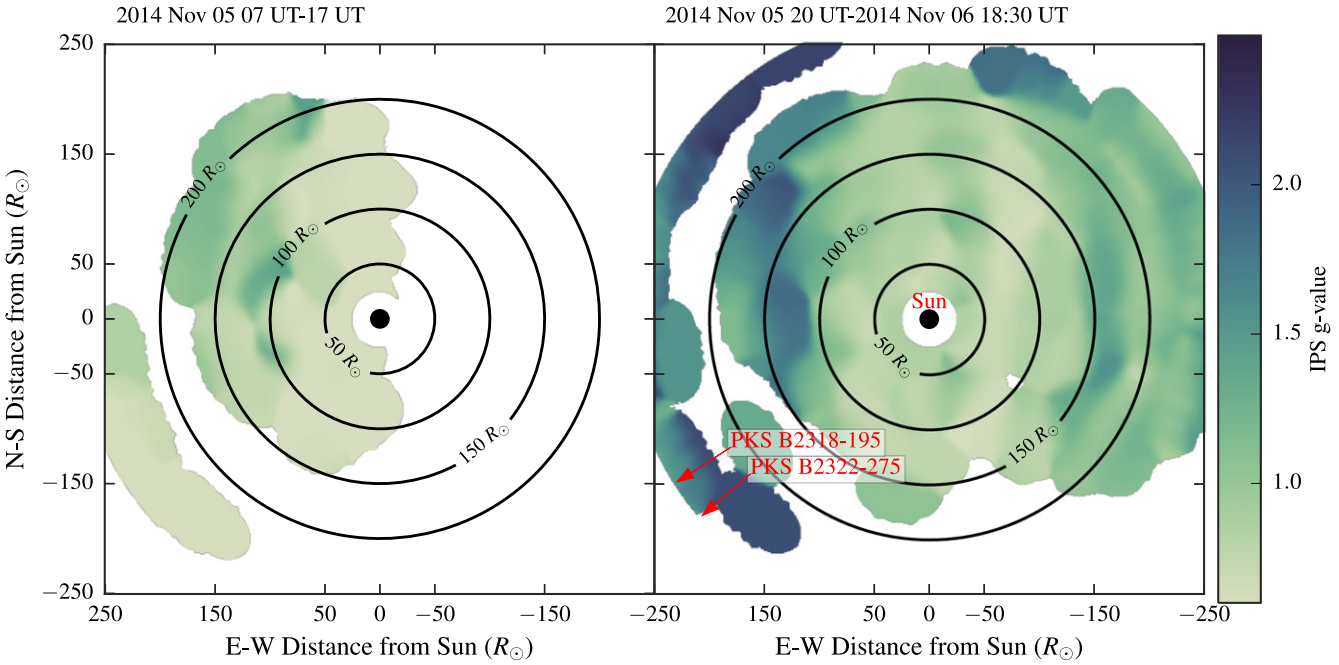

Figure 4. Ooty radio telescope 327 MHz scintillation images. Left: image for the period 2014 November 5 07 UT to 17 UT. Right: image for the period 2014 November 5 20 UT to 6 18:30 UT (which spans our scintillation event at 13:30 UT). The images show the level of scintillation measured by the g parameter (e.g., Manoharan 2010), where $g = 1$ is a normal level of turbulence. Radial distance from the center shows the derived heliocentric distance of the scattering medium: concentric circles with radii of 50, 100, 150, and 200 $R_\odot$ are plotted and labeled. North is up, and east to the left. The arrows show the directions toward PKS B2322−275 and PKS B2318−195 starting at a distance of 1 AU (215 $R_\odot$). The image from November 5 shows very little IPS, while the image from November 6 shows a significant increase in IPS toward the southeast where the MWA data are.

conditions[23] (S. T. Loi 2015, private communication). In the absence of any other viable explanation for what we see, and since what we see agrees with all of the known properties (amplitude, timescale, and source selection) of IPS (as in Hewish et al. 1964), we conclude IPS is the most likely origin of the anomalous variability. This is largely confirmed by the Ooty Radio Telescope observations.

3.2. Variability Properties

The modulation of PKS B2318−195 appears to start 20–30 minutes after that for PKS B2322−275, and that the period of enhanced modulation lasts for about 30 minutes for both sources (although some of the modulation may extend past the end of our observing period). Assuming the modulation is caused by IPS from a CME, the elongation difference implies a speed of ∼500 km s^{-1} for a distance of 0.1 AU. This speed is consistent with those inferred from Ooty observations on 2014 November 6, where a number of sources at elongations >90° that were in the same direction as PKS B2322−275 and PKS B2318−195 showed significantly enhanced scintillation (see Figure 3 for an example). For a solar wind speed of 500 v_{500} km s^{-1}, we infer a minimum transverse size of the CME of $9 \times 10^5 v_{500}$ km from the duration of the modulation. However, given typical radial expansion of CMEs (e.g., Manoharan et al. 2000) we expect radial sizes of 0.2–0.4 AU. Therefore we believe that the duration of the IPS is set by the thickness of some sub-structure within the putative CME.

As there is significant variability down to our sampling of 2 s, we infer CME structure on scales down to $\lesssim$1000 v_{500} km. We see an apparent transition from a flat power spectrum to a decline in Figure 3. This may be associated with the Fresnel scale, above which IPS is suppressed (Manoharan & Ananthakrishnan 1990). However, actually measuring the Fresnel scale and directly constraining the turbulent properties generally requires considerably faster sampling. Instead, since the rms fluctuations are <100%, it is likely that the sources are partially resolved by IPS, the change in spectral slope could have more to do more with intrinsic source sub-structure (this would be consistent with the change in scintillation with radio frequency in Figure 2).

3.3. Identification of Candidate CMEs

At the time of the observation, PKS B2322−275 was at $\epsilon = 114°$ and a position angle of about 114° (east of north). So any plasma structure that caused the scintillation would have to have been outside the orbit of the Earth and below the ecliptic (Figure 4). With typical speeds of 500–1000 km s^{-1}, we searched for CMEs that were observed to occur around 3–5 days before our observations. Among the CMEs identified by Computer Aided CME Tracking software (CACTus; Robbrecht et al. 2009) we identified a number with reasonable ejection times and angles. The scintillation image produced by the Ooty Radio Telescope (Figure 4) for 2014 November 5 up to 17:00 UT shows little scintillation in the direction toward PKS B2322−275, while the scintillation increased significantly after 20:00 UT and contiuing on 2014 November 6. Without more detailed tracking or simulation of heliospheric structures, especially beyond Earth, we cannot conclusively determine

[23] While we do see a modest enhancement in the auroral activity (given by the AE index) that peaks near 13:25 UT, the enhancement is not very notable, there are multiple enhancements that day, and there are even more significant enhancements on our comparison night which are not coincident with scintillation.

whether a specific CME or region resulting from multiple CME interactions caused the observed scintillations.

4. CONCLUSIONS

Plans for observations of IPS with the new generation of low-frequency radio telescopes, namely LOFAR and the MWA, concentrate on dedicated high-time-resolution ($\lesssim$10 ms) observations of pre-selected sources. The temporal and frequency dependence of IPS flux variations help probe the structure of the solar wind (including possible CMEs) (e.g., Oberoi & Benkevitch 2010; Bowman et al. 2013; Fallows et al. 2013). These observations are similar in strategy to dedicated programs with existing facilities like the Ooty radio telescope (Manoharan 2010), which measures scintillation of 400–800 sources each day distributed over $\epsilon < 100°$.

Assuming the variability we see is related to IPS, we have discussed a different regime. First, we used commensal nighttime observations with the MWA, so $\epsilon > 90°$. Second, the sources observed at facilities like Ooty correspond to 155 MHz flux densities $S_{155} \gtrsim 10$ Jy, which have an areal density of $\approx$100 sr^{-1} = 0.03 deg^{-2} (Williams et al. 2012). Over the 600 deg^2 MWA field of view that means we would detect at least 20 of these bright sources. In fact, we can sensitively probe flux density variations of 20% in a single 2 s integration for sources as weak as 1 Jy, which have a sky density 30$\times$ higher. Therefore, the density of sight-lines on the sky available to probe IPS is a factor of five finer, and in fact weaker sources are observed to vary (at lower confidence) along with the sources discussed here. While the 2 s integrations used here average over much of the higher-time-resolution IPS structure, quasi-real time analysis (as in Mitchell et al. 2008) can be used to identify scintillating sources which can then be followed at higher time resolution using dedicated observations (Tremblay et al. 2015).

One difficulty in interpreting our results, though, comes from the fact that we are looking outside the Earth's orbit, where the geometry does not allow easy identification of the distances to turbulent structures (cf., Armstrong & Coles 1978). Even so, we can still examine the statistics of IPS-like variability over multi-year timescales, correlating it with dedicated ground- and space-based solar observing. We can also probe the fraction of compact (<arcsec) emission from the roughly 10^4 bright, high-latitude (where scatter broadening will not matter; Cordes & Lazio 2002) sources to be observed in various MWA surveys (cf. hundreds of sources in Little & Hewish 1968; Jeyakumar et al. 2000; although see Hajivassiliou & Duffett-Smith 1990), providing a useful adjunct to calibrator surveys and allowing connections between spectral and spatial properties of sources.

Finally, we note that the existence of strong IPS in nighttime observations of a primary field for the MWA EoR experiment using nominal imaging parameters may be concerning. However, a detailed analysis by Trott & Tingay (2015) shows that under all but extreme conditions, IPS will not affect the detectability of the EoR signal.

We thank an anonymous referee for a thorough and thoughtful review. We thank B. Jackson, C. Loi, and A. Rowlinson for helpful conversations. This scientific work makes use of the Murchison Radio-astronomy Observatory, operated by CSIRO. We acknowledge the Wajarri Yamatji people as the traditional owners of the Observatory site. Support for the MWA comes from the U.S. National Science Foundation (grants AST-0457585, PHY-0835713, CAREER-0847753, and AST-0908884), the Australian Research Council (LIEF grants LE0775621 and LE0882938), the U.S. Air Force Office of Scientific Research (grant FA9550-0510247), and the Centre for All-sky Astrophysics (an Australian Research Council Centre of Excellence funded by grant CE110001020). D.L.K. is additionally supported by NSF grant AST-1412421. P.K.M. acknowledges partial support from ISRO. Support is also provided by the Smithsonian Astrophysical Observatory, the MIT School of Science, the Raman Research Institute, the Australian National University, and the Victoria University of Wellington (via grant MED-E1799 from the New Zealand Ministry of Economic Development and an IBM Shared University Research Grant). The Australian Federal government provides additional support via the Commonwealth Scientific and Industrial Research Organisation (CSIRO), National Collaborative Research Infrastructure Strategy, Education Investment Fund, and the Australia India Strategic Research Fund, and Astronomy Australia Limited, under contract to Curtin University. We acknowledge the iVEC Petabyte Data Store, the Initiative in Innovative Computing and the CUDA Center for Excellence sponsored by NVIDIA at Harvard University, and the International Centre for Radio Astronomy Research (ICRAR), a Joint Venture of Curtin University and The University of Western Australia, funded by the Western Australian State government. This research made use of APLpy, an open-source plotting package for Python hosted at http://aplpy.github.com.

Facilities: Murchison Widefield Array, Ooty Radio Telescope.

REFERENCES

Armstrong, J. W., & Coles, W. A. 1978, ApJ, 220, 346
Bell, M. E., Murphy, T., Kaplan, D. L., et al. 2014, MNRAS, 438, 352
Bisi, M. M., Fallows, R. A., Jensen, E. A., et al. 2011, in AGU Fall Meeting 2011, abstract SH31C–2020
Bowman, J. D., Cairns, I., Kaplan, D. L., et al. 2013, PASA, 30, 31
Chhetri, R., Ekers, R. D., Jones, P. A., & Ricci, R. 2013, MNRAS, 434, 956
Clarke, M. 1964, PhD thesis, Cambridge Univ.
Coles, W. A. 1978, SSRv, 21, 411
Cordes, J. M., & Lazio, T. J. W. 2002, arXiv:astro-ph/0207156
Cordes, J. M., & Rickett, B. J. 1998, ApJ, 507, 846
Culhane, J. L., Harra, L. K., James, A. M., et al. 2007, SoPh, 243, 19
Eyles, C. J., Harrison, R. A., Davis, C. J., et al. 2009, SoPh, 254, 387
Fallows, R. A., Asgekar, A., Bisi, M. M., Breen, A. R., & ter-Veen, S. 2013, SoPh, 285, 127
Fallows, R. A., Coles, W. A., McKay-Bukowski, D., et al. 2014, JGRA, 119, 10544
Hajivassiliou, C. A., & Duffett-Smith, P. J. 1990, MNRAS, 247, 491
Hancock, P. J., Murphy, T., Gaensler, B. M., Hopkins, A., & Curran, J. R. 2012, MNRAS, 422, 1812
Hewish, A., Bell, S. J., Pilkington, J. D. H., Scott, P. F., & Collins, R. A. 1968, Natur, 217, 709
Hewish, A., Scott, P. F., & Wills, D. 1964, Natur, 203, 1214
Hurley-Walker, N., Morgan, J., Wayth, R. B., et al. 2014, PASA, 31, 45
Jackson, B. V., Hick, P. L., Kojima, M., & Yokobe, A. 1998, JGR, 103, 12049
Jeyakumar, S., Saikia, D. J., Pramesh Rao, A., & Balasubramanian, V. 2000, A&A, 362, 27
Kojima, M., & Kakinuma, T. 1990, SSRv, 53, 173
Little, L. T., & Hewish, E. 1968, MNRAS, 138, 393
Loi, S. T., Murphy, T., Bell, M. E., et al. 2015b, MNRAS, submitted
Loi, S. T., Murphy, T., Cairns, I. H., et al. 2015a, GeoRL, 42, 3707
Lonsdale, C. J., Cappallo, R. J., Morales, M. F., et al. 2009, IEEEP, 97, 1497
Lorimer, D. R., Bailes, M., McLaughlin, M. A., Narkevic, D. J., & Crawford, F. 2007, Sci, 318, 777
Manoharan, P. K. 2010, SoPh, 265, 137
Manoharan, P. K., & Ananthakrishnan, S. 1990, MNRAS, 244, 691

Manoharan, P. K., Kojima, M., Gopalswamy, N., Kondo, T., & Smith, Z. 2000, ApJ, 530, 1061
McCarthy, P. J., Kapahi, V. K., van Breugel, W., et al. 1996, ApJS, 107, 19
Mejia-Ambriz, J. C., Villanueva-Hernandez, P., Gonzalez-Esparza, J. A., Aguilar-Rodriguez, E., & Jeyakumar, S. 2010, SoPh, 265, 309
Mitchell, D. A., Greenhill, L. J., Wayth, R. B., et al. 2008, ISTSP, 2, 707
Murphy, T., Sadler, E. M., Ekers, R. D., et al. 2010, MNRAS, 402, 2403
Oberoi, D., & Benkevitch, L. 2010, SoPh, 265, 293
Offringa, A. R., McKinley, B., Hurley-Walker, N., et al. 2014, MNRAS, 444, 606
Readhead, A. C. S. 1994, ApJ, 426, 51
Rickett, B. J. 1986, ApJ, 307, 564
Robbrecht, E., Berghmans, D., & van der Linden, R. A. M. 2009, ApJ, 691, 1222
Schou, J., Scherrer, P. H., Bush, R. I., et al. 2012, SoPh, 275, 229
Slee, O. B. 1995, AuJPh, 48, 143
Sutinjo, A., O'Sullivan, J., Lenc, E., et al. 2015, RaSc, 50, 52
Thompson, A. R., Moran, J. M., & Swenson, G. W., Jr. 2001, Interferometry and Synthesis in Radio Astronomy (2nd ed.; New York: Wiley)
Thornton, D., Stappers, B., Bailes, M., et al. 2013, Sci, 341, 53
Tingay, S. J., Goeke, R., Bowman, J. D., et al. 2013, PASA, 30, 7
Tingay, S. J., Trott, C. M., Wayth, R. B., et al. 2015, AJ, submitted
Tokumaru, M., Kojima, M., Fujiki, K., Yamashita, M., & Yokobe, A. 2003, JGRA, 108, 1220
Tokumaru, M., Kojima, M., Fujiki, K., et al. 2011, RaSc, 46, 0
Tremblay, S. E., Ord, S. M., Bhat, N. D. R., et al. 2015, PASA, 32, 5
Trott, C., & Tingay, S. J. 2015, ApJ, submitted
van Haarlem, M. P., Wise, M. W., Gunst, A. W., et al. 2013, A&A, 556, A2
Williams, C. L., Hewitt, J. N., Levine, A. M., et al. 2012, ApJ, 755, 47